Available online at www.sciencedirect.com
ScienceDirect
Trans. Nonferrous Met. Soc. China 32(2022) 307−318

Transactions of
Nonferrous Metals
Society of China
www.tnmsc.cn

Features and mechanisms of self-sintering of molybdenite during oxidative roasting

Hu SUN[1,2], Guang-hui LI[1,2], Qun-zhen BU[1,2], Zhong-qiao FU[1,2],
Hui-bo LIU[1,2], Xin ZHANG[1,2], Jun LUO[1,2], Ming-jun RAO[1,2], Tao JIANG[1,2]

1. School of Minerals Processing and Bioengineering, Central South University, Changsha 410083, China;
2. National Engineering Laboratory for High Efficiency Recovery of Refractory Nonferrous Metals,
Changsha 410083, China

Received 21 November 2020; accepted 10 August 2021

Abstract: Roasting experiments were carried out with pure reagents as raw materials. The self-sintering behaviors of molybdenite (MoS_2) during oxidation were investigated by thermodynamic calculation, XRD, SEM-EDS and high-temperature in situ analysis. The results indicate that the desulfurization efficiency of MoS_2 pellet decreases with the increase of roasting temperature from 600 to 700 °C, owing to the expansion of sintered area. At the very beginning of roasting, sintered layer can be rapidly formed and cover the pellet surface on the windward side, and meanwhile, MoO_2 and Mo_4O_{11} intensively appear and constitute the sintered layer together with MoO_3. Moreover, it is proven that MoO_3-rich products containing low-valence molybdenum oxides have low melting points, thus easy to be melted during the occurrence of exothermic reaction between MoS_2 and O_2, which leads to the sintering of materials.

Key words: molybdenite; oxidative roasting; sintering; distribution characteristic; mechanism

---

1 Introduction

Molybdenite (MoS_2) concentrates are the basic raw materials of molybdenum metallurgy. Most of MoS_2 concentrates are oxidized into technical-grade molybdic oxide (MoO_3) first, which is a vital intermediate material for preparing ferro-molybdenum [1,2], ammonium molybdates [3,4], and sublimed pure MoO_3 [5,6]. The oxidation of MoS_2 concentrates is mainly performed through two routes: oxygen-pressure digestion [7] and oxidative roasting [4]. Comparatively, the fire method can achieve larger production capacity, whereas hydrometallurgical method is superior in less energy consumption and environmental pollution [8].

China is the largest producer and consumer of molybdenum in the world [9]. The large consumption demand for Mo-containing steels urges most of firms to employ fire method to process MoS_2 concentrates [10]. For the roasting process, the oxidation efficiency determines the length of heating period, the concentration of SO_2 in flue gas, and the chemical composition of roasted ore, thereby affecting the energy consumption, the cost of acid making using flue gas [11], and the adaptability of product for further processing. Among several roasting methods, fluidized bed roasting has the highest oxidation efficiency [12], but suffers from high dust removal of over 40% [13], and complex operation and equipment. Consequently, moving bed roasting using rotary kiln or multiple-hearth furnace has become the mainstream method because of easy operation and simple equipment [10,11]. However, the mainstream

---

Corresponding author: Guang-hui LI, Tel: +86-731-88830542, E-mail: liguangh@csu.edu.cn;
Jun LUO, Tel: +86-731-88830542, E-mail: luojun2013@csu.edu.cn

DOI: 10.1016/S1003-6326(22)65796-0

method also has several shortcomings: roasting a batch of molybdenite concentrates commonly requires a long period of 2−5 h at temperatures of 550−700 °C [4]; the roasted ore still contains much MoO_2 that is insoluble in ammonia water; the concentration of SO_2 in flue gas is only 1%−2%, which is too low for cost-effective acid making [11].

So far, a considerable amount of work on oxidation process of MoS_2 has been reported. It is confirmed that MoS_2 oxidation conforms to the unreacted shrinking nucleus model [14−16]. The oxidation of MoS_2 particle starts from the surface to inner core. With time extending, the oxidized layer gradually thickens, which inhibits the inner MoS_2 from contacting O_2, so the inner diffusion of O_2 becomes the rate-limiting step most of time [15,16]. Besides, the high-temperature sintering of MoS_2 concentrate is also a significant reason for low oxidation efficiency. LI et al [17] report that low-grade MoS_2 concentrate will be seriously sintered at 600 °C unless it is pre-purified. SUN et al [18,19] find that MoS_2 concentrate added with 20% $CaCO_3$ is densely sintered at 775 °C, and high-grade MoS_2 concentrate roasted at over 800 °C sticks together due to liquid sintering. WANG et al [20] investigate the effects of different impurities on the agglomeration of MoS_2 concentrate, and confirm that impurities of K, Cu, Pb, and Fe can increase the extent of agglomeration due to the formation of low-melting-point eutectics. In addition, it is also reported that MoS_2 concentrate is more likely to be sintered in pure O_2 atmosphere [21,22].

Overall, in prior research, the effects of impurities, temperature, and atmosphere on the sintering of MoS_2 concentrates have been clarified to some extent. However, there is hardly systematic research about the sintering of pure MoS_2. As the major component in molybdenum ore, MoS_2 may be self-sintered at high temperatures, which should be mostly responsible for the poor oxidation rate. Besides, little attention has been paid to the formation time and spatial distribution of sintered layer, but these factors are important because they may help to create response measures. In this work, the feasibility of MoS_2 oxidation reactions was verified based on thermodynamic calculations. The rules of desulfurization efficiency, mass loss, and phase transformation of MoS_2 under various conditions were revealed. The structure, distribution, and composition of sintered layer were ascertained, Further, the exothermic effect of MoS_2 oxidation and melting characteristics of MoO_3-rich systems containing MoO_2 and Mo_4O_{11} were figured out. Generally, this work has provided a comprehensive analysis of the features and mechanisms of self-sintering of MoS_2, which may help to find out some solutions to the current problem.

2 Experimental

2.1 Materials

Hexagonal-phase MoS_2 (99.5%, Aladdin) was used as the mineral of molybdenite for oxidative roasting. Pure Mo (99.9%, Aladdin) and pure MoO_3 (99.9%, Aladdin) were used to synthesize the oxides of low valence states of Mo. High-purity N_2 (99.999 vol.%) was also used to protect samples from being oxidized.

2.2 Oxidative roasting of MoS_2 pellet

Pure MoS_2 was ground in an agate mortar for 5 min, and dry-pressed into small pellets with a stainless-steel mold (*d*6 mm × 6 mm) under a pressure of 5 MPa. After forming, each pellet was about 6 mm in height and weighed about 0.3 g.

Oxidative roasting was performed via the set-up in Fig. 1. The MoS_2 pellet was placed on a quartz substrate and then steadily pushed into the heating zone of tube furnace under the protection of N_2 flow of 2 L/min. Once the temperature stabilized, inert gas was changed to air flow (2 L/min), and oxidation process started. After certain period, air was changed back to N_2, and then the roasted pellet was pulled out to low-temperature zone for cooling.

The temperature of MoS_2 pellet during roasting was measured via a thermocouple with an

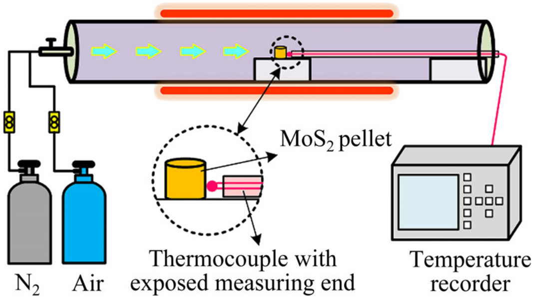

Fig. 1 Schematic diagram of set-up for roasting MoS_2 pellet and measuring pellet temperature

exposed measuring end, which improved the precision and sensitivity. The thermocouple was placed with measuring end touching the pellet surface. The temperature was automatically recorded once per second via a recorder.

2.3 Characterization of melting characteristics of mixed molybdenum oxides

MoO_2 and Mo_4O_{11} were synthesized via solid−solid reactions. Two mixtures composed of pure MoO_3 and pure Mo were proportioned in molar ratios of 2:1 and 11:1, and evenly mixed by wet grinding for 30 min, corresponding to the precursors of MoO_2 and Mo_4O_{11}, respectively. The precursors were dry-pressed into pellets with a pressure of 30 MPa, heated at 700 °C for 6 h under N_2 protection, and finally crushed into powders after cooling down.

Melting points of MoO_3−MoO_2 and MoO_3−Mo_4O_{11} systems were measured with a high-temperature in situ analyzer (S/DHTT-TA-III, Chongqing University, China) [23]. Each mixture was ground in alcohol for 10 min to obtain a uniform slurry, then added to a U-type Pt−Rh thermocouple wire with an amount of 1−3 mg, and finally put into the heating furnace by a feeder. The heating rate was controlled at 5 °C/s, and the heating chamber was continuously supplied with N_2 flow. In each second, the camera joined with the microscope captured four pictures of the heated sample, which were used to judge the melting characteristics.

2.4 Instruments

Phases of roasted pellets were identified via an X-ray diffraction (XRD, D/Max 2500, RIGAKU, JPN) under the conditions: Cu K_{α}; tube current and voltage, 250 mA and 40 kV; scanning range, 5°−80° (2θ); step size, 0.02° (2θ); scanning speed, 5 (°)/min. Sulfur contents in roasted pellets were measured using infrared carbon−sulfur analyzer (Leco Corporation, CS844). The microstructures and compositions of samples were investigated with scanning electron microscopy (SEM, MIRA3, Tescan, CZ) equipped with an energy dispersive X-ray (EDX) spectroscope. The images were recorded in backscatter electron mode operated at a low vacuum of 66.65 Pa and 10 keV. Thermodynamic calculations were performed with "HSC Chemistry 9" using "Reaction Equations" and "Stability Diagrams" modules, and all data such as standard enthalpy changes and heat capacities were originated from the software itself.

3 Results and discussion

3.1 Reaction thermodynamics of MoS_2 during oxidative roasting

Predominance diagrams for Mo−O−S system at 550 and 700 °C are shown in Fig. 2. The oxidation of MoS_2 to the target product MoO_3 at 550 °C only requires a minimum O_2 partial pressure of $10^{-8.3}$ kPa. With a higher temperature of 700 °C, the required O_2 pressure slightly increases to $10^{-5.7}$ kPa. In practice, O_2 pressure in flue gas of rotary kiln can reach 15−20 kPa, which is far larger than the theoretical value for producing MoO_3. However, it is often the case that MoS_2 particles are wrapped by newly produced MoO_3, and thus cannot be exposed to O_2. Hence, low-valence molybdenum oxides, such as MoO_2, Mo_4O_{11}, Mo_8O_{23}, and Mo_9O_{26} may be produced.

Possible reactions of MoS_2 oxidation into MoO_2, Mo_4O_{11} and MoO_3 are summarized in Reactions (1)−(6). Ideally, powdery MoS_2 exposed

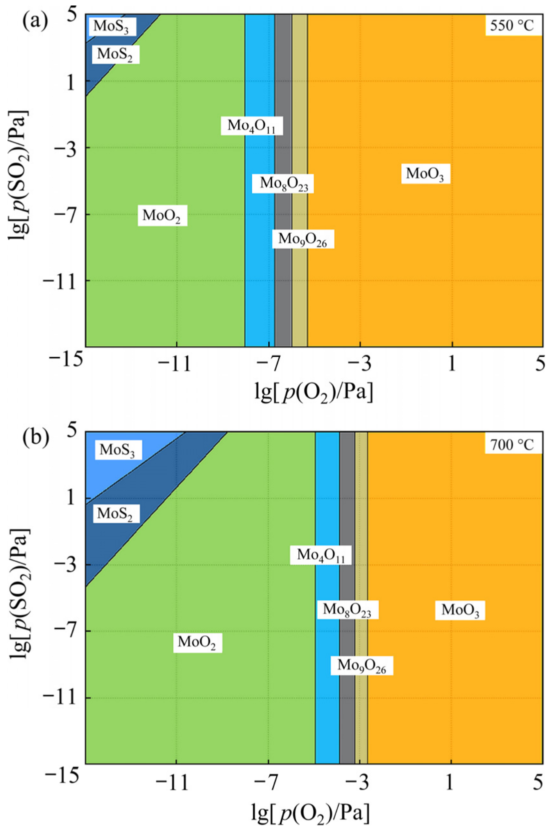

Fig. 2 Predominance diagrams for Mo−O−S systems at 550 °C (a) and 700 °C (b)

in air can be directly oxidized into MoO_3 via Reaction (1) [24]. MoS_2 wrapped by MoO_3 can be transformed into MoO_2 and Mo_4O_{11} via Reactions (2) and (3), respectively. Mo_4O_{11} can also be produced via solid−solid Reaction (4) between MoO_3 and MoO_2. MoO_2 and Mo_4O_{11} can further react with O_2 that is supplied by inner diffusion to produce MoO_3. Feasibilities of these reactions are verified from the perspective of thermodynamics, as shown in Fig. 3. The results indicate that all the reactions can occur in theory. Comparatively, Reactions (1)−(3) with SO_2 producing have greater occurrence tendency, while solid−solid reaction (Reaction (4)) has the lowest tendency.

$$MoS_2+3.5O_2(g)=MoO_3+2SO_2(g) \tag{1}$$

$$MoS_2+6MoO_3=7MoO_2+2SO_2(g) \tag{2}$$

$$MoS_2+27MoO_3=7Mo_4O_{11}+2SO_2(g) \tag{3}$$

$$MoO_2+3MoO_3=Mo_4O_{11} \tag{4}$$

$$MoO_2+1/2O_2(g)=MoO_3 \tag{5}$$

$$Mo_4O_{11}+1/2O_2(g)=4MoO_3 \tag{6}$$

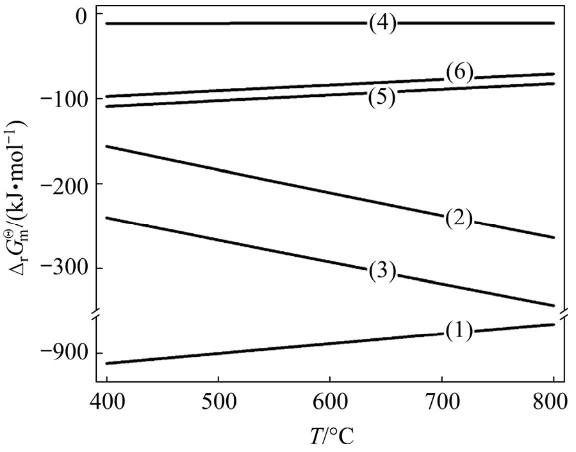

Fig. 3 Standard Gibbs free energy changes ($\Delta_r G_m^\ominus$) of Reactions (1)−(6) in temperature range of 400−800 °C

3.2 Changes in sulfur content and mass change of MoS_2 pellets during oxidative roasting

Desulfurization efficiencies of MoS_2 pellets roasted at different temperatures for varying periods were measured, as depicted in Fig. 4(a). When MoS_2 pellets are roasted at 600 °C, the desulfurization efficiency rapidly increases up to 95.7% within 10 min, and reaches 99.0% within 20 min. Further raising the temperature only succeeds in decreasing the oxidation speed. Specifically, it takes 40 min at 650 °C or 60 min at 700 °C to remove 99% of sulfur. Prior research reported that the oxidation of MoS_2 powder can be accelerated by increasing the temperature from 505 to 565 °C [15]. However, when pelletized MoS_2 is roasted at temperatures as high as 650 and 700 °C, the oxidation regularity is reversed.

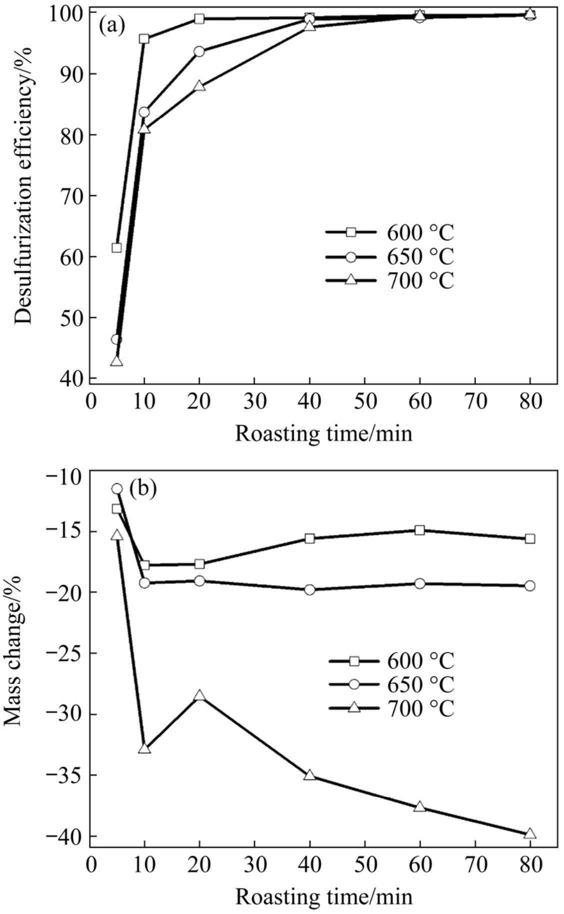

Fig. 4 Desulfurization efficiency (a) and mass change (b) of MoS_2 pellets during oxidative roasting at different temperatures

The mass change of MoS_2 pellets roasted at different temperatures for varying periods was also measured, as shown in Fig. 4(b). The mass change of MoS_2 pellet rapidly decreases in the first 10 min, and then slightly increases in the period of 10−20 min. With time further extending, the pellet roasted at 600 °C has a slight mass increase of 2%−3%; the pellet roasted at 650 °C maintains a mass change of 19%−20%; the pellet roasted at 700 °C has a sharp mass decrease of over 10%. After 80 min, mass losses of pellets roasted at 600, 650, and 700 °C reach 15.6%, 19.5%, and 39.9%, respectively. Among the reactions listed above, Reactions (1)−(3) can result in mass loss, whereas Reactions (5) and (6) can lead to mass increase. Based on this, reasons for mass changes in different periods may be figured out. For example, the mass increase of pellet in the period of 10−20 min may result from the oxidation of MoO_2 and Mo_4O_{11}, which are produced in the first 10 min. Besides, it is noticed that the mass loss of pellet roasted at 700 °C far exceeds the theoretical maximum of 20.1% that can be achieved when MoS_2 is totally transformed into MoO_2, indicating that mass loss derived from MoO_3 volatilization is also significant at high temperatures [18,25].

3.3 Phase transformation of MoS_2 pellets during oxidative roasting

Phase compositions of pellets roasted at different temperatures for varying periods were identified, as displayed in Figs. 5(a−c). When the pellet is roasted at 600 °C, only a small amount of MoS_2 exists after 10 min, and the MoS_2 almost disappears after 20 min. However, the MoS_2 cannot disappear in 20 min when roasted at 650 °C. Moreover, it takes more than 40 min to oxidize the MoS_2 pellet at a higher temperature of 700 °C.

The oxidation products contain certain amount of MoO_2. According to the standard PDF card No.78-1069, the strongest diffraction peak of MoO_2 is around 26.0° (2θ). Herein, XRD patterns near the position of 26.0° (2θ) are enlarged, as shown in Figs. 5(d−f). It is found that MoO_2 is intensively formed in the first 5 min at high temperatures of 650 and 700 °C. The MoO_2 can be gradually

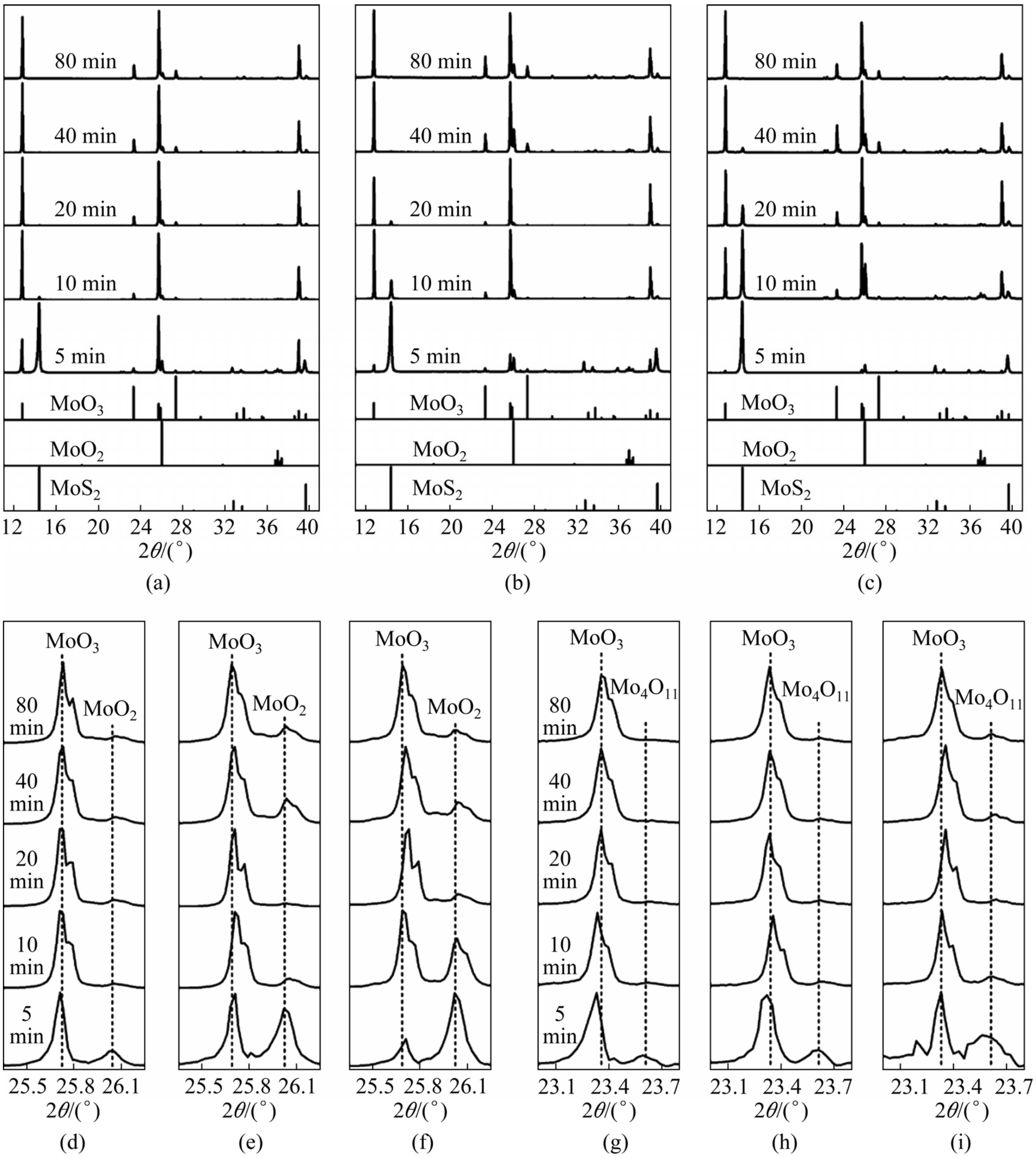

Fig. 5 XRD patterns (a−c), and enlarged XRD patterns focusing on MoO_2 (d−f) and Mo_4O_{11} (g−i) diffraction peaks of MoS_2 pellets roasted at 600 °C (a, d, g), 650 °C (b, e, h) and 700 °C (c, f, i)

oxidized over time, but the oxidation speed is very slow. After 80 min, the remaining MoO_2 may either be the initially-formed MoO_2 that is not further oxidized at later stages, or be the newly-formed MoO_2 at later stages.

Prior research reported that Mo_4O_{11} is an intermediate product of hydrogen reduction of MoO_3 [26], and herein thermodynamic calculations also indicated that Mo_4O_{11} may be formed via Reactions (3) and (4). According to the standard PDF card No.84-0687, the strongest diffraction peak of Mo_4O_{11} is at about 23.6° (2θ). Enlarged XRD patterns focusing on the strongest Mo_4O_{11} diffraction peak are displayed in Figs. 5(g−i). It is seen that Mo_4O_{11} also tends to be formed in the initial period of high-temperature roasting, but its content may be much lower than that of MoO_2. The similar formation regularities of MoO_2 and Mo_4O_{11} may be ascribed to the occurrence of Reaction (4), that is, the formation of MoO_2 also promotes the formation of Mo_4O_{11}.

The formation of MoO_2 and Mo_4O_{11} indicates that some MoS_2 particles inside the pellet cannot directly react with O_2. Although the green MoS_2 pellets contain many inner pores, the sintering of materials can block the paths for O_2 diffusion, resulting in the formation of MoO_2 and Mo_4O_{11}. Besides, the sintering of materials may be more serious at higher temperatures, so MoO_2 and Mo_4O_{11} are easily formed at over 650 °C.

3.4 Microstructure and phase distribution in roasted pellets

MoS_2 pellet roasted at 600 °C for 5 min was observed via SEM, as shown in Fig. 6. The image of overall cross-section of pellet (Fig. 6(a)) shows that the oxidation layer (white area) is distributed unevenly along the circumference. Interestingly, the surface coated with a thin oxidation layer (40−60 μm) is the windward side, whereas the surface coated with a thick oxidation layer (1 mm) is the leeward side (Fig. 6(b)). On the leeward side, the oxidation layer is highly porous, and the oxidation interface close to un-oxidized MoS_2 core is loose (Fig. 6(c)). Comparatively, on the windward side, the oxidation layer is much denser. The big difference between the windward side and leeward side is the oxygen content. In existing research, O_2-enriched air and pure O_2 have been used to oxidize MoS_2 concentrates, but the oxidation efficiency does not turn better [21]. Herein, it is proven that even under the conditions of air atmosphere and a low roasting temperature of 600 °C, the MoS_2 on the windward side is still poorly oxidized due to the formation of sintered surface.

Intuitively, there are phases with three or four different grey levels in the surface layer of pellet. The EDS line scan results (Fig. 6(d)) show that, from the pellet surface to the oxidation interface, O content decreases in three stages while Mo content increases roughly in two stages. EDS results for micro-areas (1−6) in Figs. 6(e) and (f) further reveal the compositions of each layer: the outermost layer is composed of MoO_3; the middle layer consists of MoO_2 and Mo_4O_{11}; the inner layer close to the oxidation interface contains MoO_2 and MoS_2. Compared with outer oxidation layer, the inner oxidation layer close to MoS_2 core (Fig. 6(f)) is more densely sintered.

The pellet roasted at 700 °C for 5 min was also observed, as shown in Fig. 7. This pellet has a larger sintered area on the windward side (Fig. 7(a)), which is about twice as large as that of pellet roasted at 600 °C. The oxidation layer on the windward side is very dense due to serious sintering, and the outermost layer consisting of MoO_3 is only 5−10 μm thick due to the volatilization (Figs. 7(b) and (c)). On the leeward side, the oxidation layer is thick and porous (Fig. 7(d)), and the oxidation interface is loose (Fig. 7(e)). However, it is seen that some MoS_2 coated with sintered layer also locally appears on the leeward side, and the oxidation layer contains hardly any MoO_3 (Figs. 7(d) and (f)). Even though the volatilization of MoO_3 can help to shorten the paths for O_2 diffusion to the oxidation interface, the oxidation efficiency is very low due to the reinforcement of surface sintering. Overall, the MoS_2 pellet roasted at 700 °C can form large-area sintered surface on both the windward and the leeward sides, which is so dense that O_2 can hardly penetrate, so oxidation of inner Mo_4O_{11}, MoO_2 and MoS_2 is significantly hindered.

3.5 Exothermic effect of MoS_2 during oxidative roasting

The sintering of MoS_2 pellet results from the generation of liquids at high temperatures. Although temperatures of 600−700 °C are not high enough to

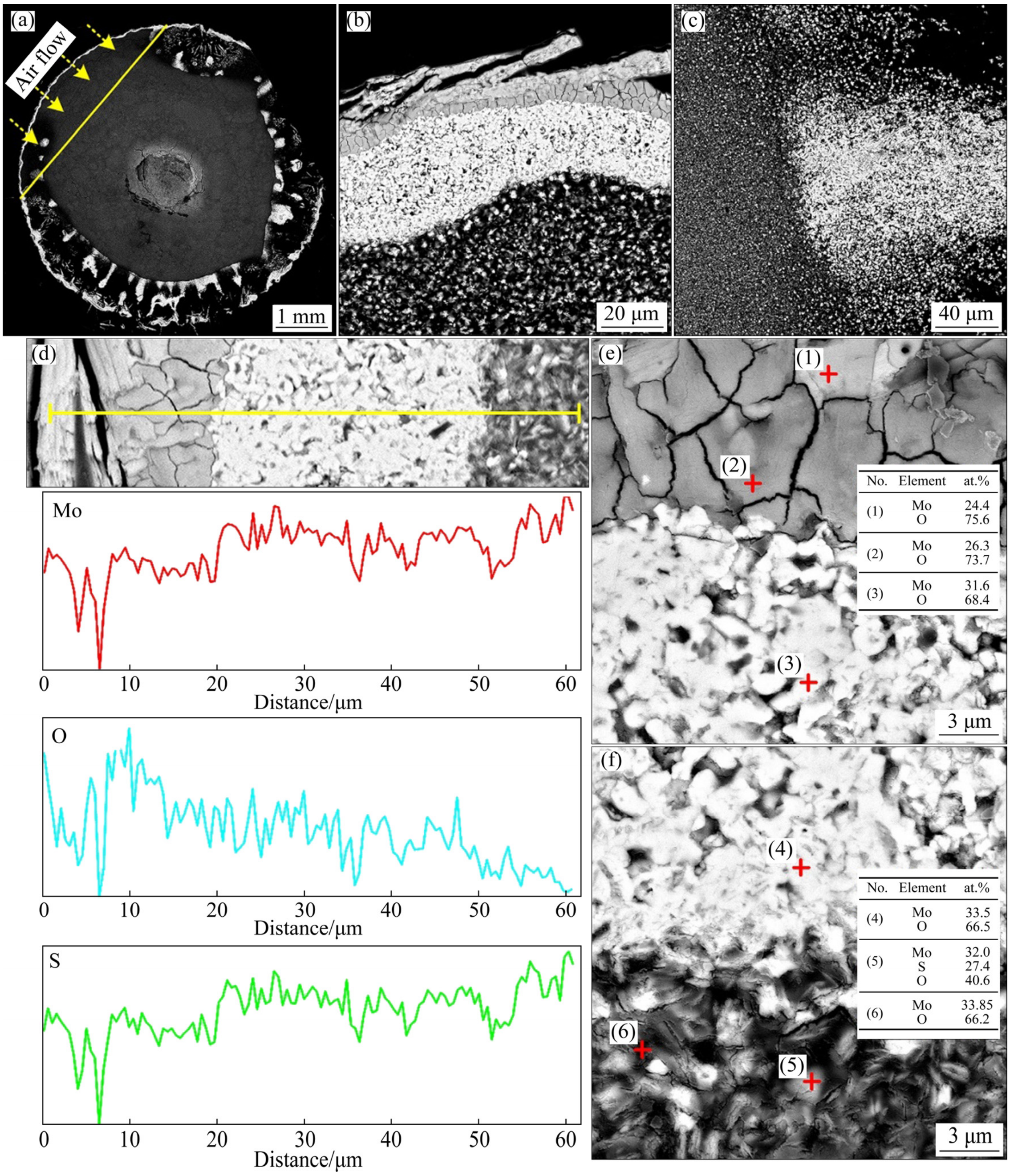

No.	Element	at.%
(1)	Mo O	24.4 75.6
(2)	Mo O	26.3 73.7
(3)	Mo O	31.6 68.4

No.	Element	at.%
(4)	Mo O	33.5 66.5
(5)	Mo S O	32.0 27.4 40.6
(6)	Mo O	33.85 66.2

Fig. 6 SEM-EDS analysis for MoS_2 pellet roasted at 600 °C for 5 min: (a) SEM image of overall cross-section of pellet; (b) SEM image of surface layer on windward side; (c) SEM image of oxidation interface on leeward side; (d) EDS line scan results for Mo, O and S elements on windward side; (e, f) Magnified SEM images of surface layer on windward side and EDS analysis results for micro-areas

melt MoO_3, the exothermic effect of oxidation reactions may help to make a great difference. Figure 8(a) displays the enthalpy changes of Reactions (1)−(6) in the temperature range of 400−800 °C. It is seen that raising the temperature cannot evidently change the enthalpy changes of these reactions. When the temperature is 600 °C, Reactions (1), (5) and (6) with MoO_3 formation can release heat of about 1058, 154, and 141 kJ/mol, respectively, while Reactions (3) and (4) with Mo_4O_{11} formation will release heat of about 68 and 13 kJ/mol, respectively. Interestingly, Reaction (2) with MoO_2 formation is an endothermic process, and can absorb heat of about 23 kJ/mol of at 600 °C. Specific heat capacities of the reactants and products at different temperatures are depicted in Fig. 8(b). Generally, these substances all have low specific heat capacities that are even less than

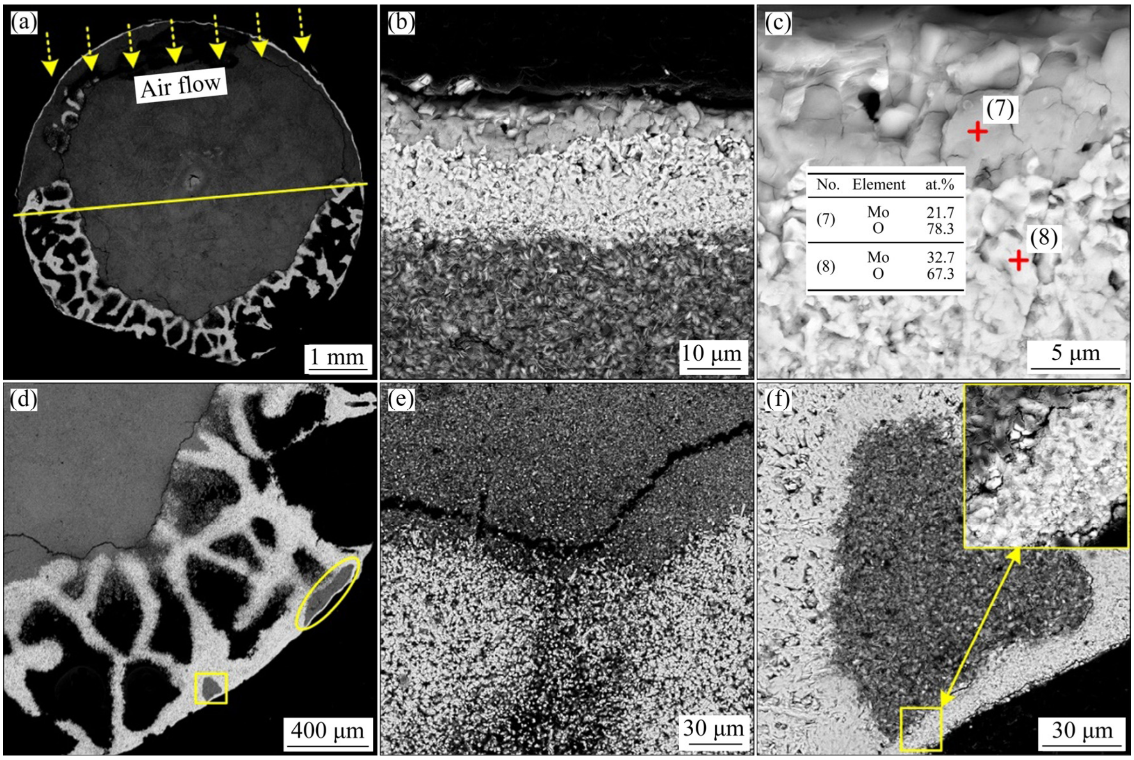

No.	Element	at.%
(7)	Mo O	21.7 78.3
(8)	Mo O	32.7 67.3

Fig. 7 SEM-EDS analysis for MoS_2 pellet roasted at 700 °C for 5 min: (a) SEM image of overall cross-section of pellet; (b) SEM image of surface layer on windward side; (c) EDS analysis results for micro-areas; (d) SEM image of outer layer on leeward side; (e) SEM image of oxidation interface on leeward side; (f) SEM image of surface layer on leeward side

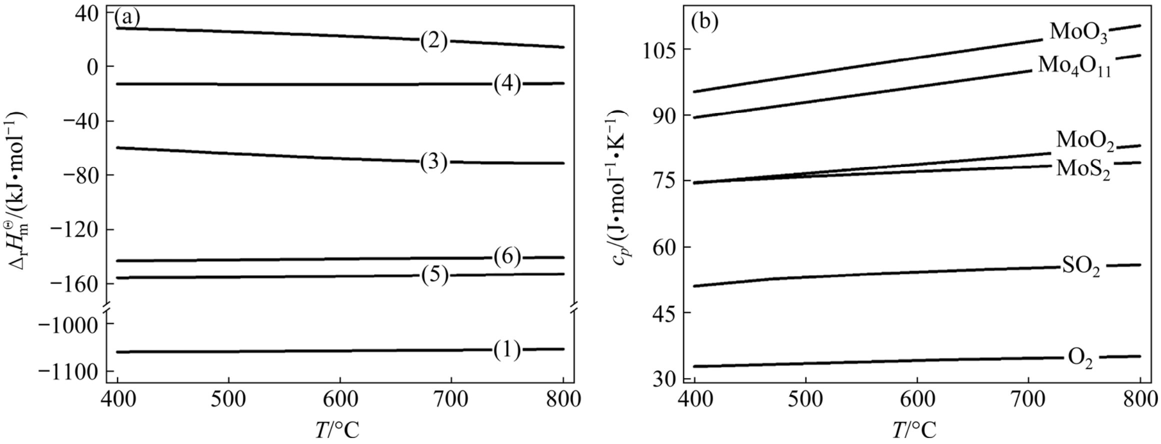

Fig. 8 Standard enthalpy changes ($\Delta_r H_m^\ominus$) of oxidation reactions of MoS_2 (a), and specific heat capacities (c_p) of reactants and products (b) in temperature range of 400−800 °C

1/10000 of the heat released by Reaction (1). Hence, the surface MoS_2 exposed in air actually has a very high temperature during oxidative roasting.

The temperature of MoS_2 pellet during oxidative roasting was measured, as shown in Fig. 9. For each test, the heating furnace was controlled at fixed temperatures of 600, 650 and 700 °C, respectively. In the first 3 min, pellets were roasted in N_2 flow. From 4 min, N_2 flow was changed to air flow. In the oxidative atmosphere, pellet temperature quickly reaches peak value at over 50 °C/min, indicating that Reaction (1) drastically occurs. In the next 2 min, pellets roasted at 650 and 700 °C have a sharp temperature drop by 25−30 °C because of the melting of solids and the endothermic effect derived from Reaction (2); while the pellet roasted at 600 °C has a small temperature drop by about 2 °C and then reaches a new temperature peak of 656.9 °C, owing to the slight sintering of pellet surface and the continuous proceeding of Reactions (1), (5) and (6). With time extending, the heat lost to the atmosphere turns to exceed the heat released from oxidation reactions, so pellet temperatures slightly drop. After 28 min, the pellet roasted at 600 °C almost has the same temperature with the heating furnace, indicating a complete oxidation, while the pellet roasted at 650 or 700 °C has a higher temperature than that of the furnace because the remaining MoS_2 is still being oxidized.

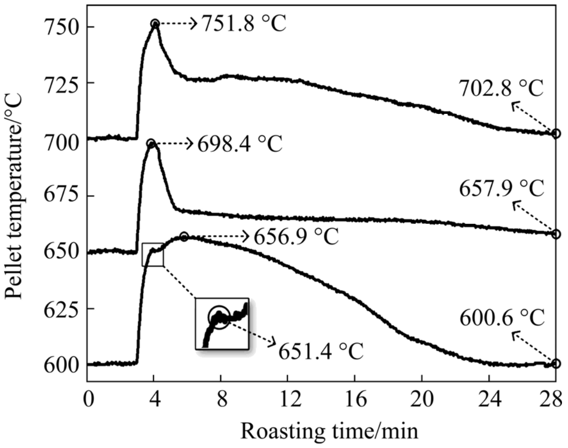

Fig. 9 Changes in temperature of MoS_2 pellet with time of oxidative roasting

According to above results, it is confirmed that the sintering of MoS_2 pellet occurs at the very early stage of oxidative roasting and can continuously inhibit the oxidation of MoS_2 in later stages. Once MoS_2 is exposed to air at high temperatures, the exothermic effect of oxidation reaction is remarkable, leading to a significant increase in local temperature. Moreover, the local temperature of MoS_2 surface that is being oxidized is likely to be much higher than the temperature peaks shown in Fig. 9, because much heat has been lost to ambient atmosphere before it is transferred to the measuring end of thermocouple. The practical temperature of pellet surface on the windward side must be high enough to form liquid MoO_3. The liquid MoO_3 penetrates the inner cracks, binds solid particles, and reacts with MoS_2 to produce the densely sintered layer composed of MoO_2 and Mo_4O_{11}. Comparatively, the temperature of pellet surface on the leeward side is not high enough to form liquids due to slow oxidation, so pores in the oxidation layer do not disappear and can still serve as paths for O_2 diffusion.

3.6 Melting characteristics of mixed molybdenum oxides

Previous results show that MoO_2 and Mo_4O_{11} are intensively formed at early stage of oxidative roasting, and co-exist with MoO_3 in oxidation layer. Herein, MoO_2 and Mo_4O_{11} have been synthesized via solid−solid reactions between MoO_3 and Mo. From Fig. 10, it is seen that XRD patterns of synthetic products are quite consistent with the standard PDF cards, and no visible peaks related to impurities are found, demonstrating that synthetic MoO_2 and Mo_4O_{11} are relatively pure.

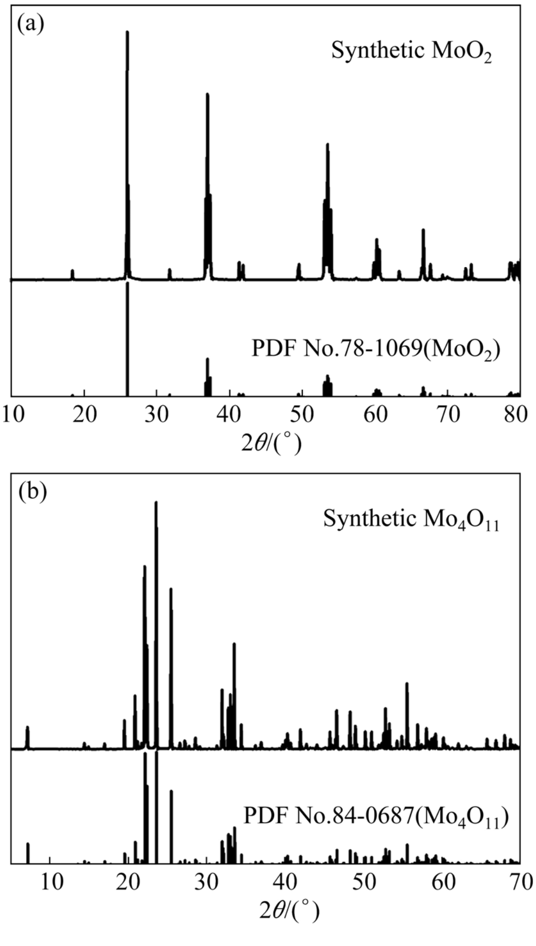

Fig. 10 XRD patterns of synthetic MoO_2 (a) and Mo_4O_{11} (b), compared with their standard PDF cards

The melting characteristics of MoO_3−MoO_2 and MoO_3−Mo_4O_{11} were measured using the high-temperature in situ analyzer equipped with a microscope. Representative images of pure MoO_3 during heating are shown in Fig. 11. As the temperature reaches 710 °C, pure MoO_3 starts to recrystallize as strip-like or flake-like orthorhombic crystals. The MoO_3 crystals will grow larger and luxuriant with temperature increasing, and completely turn into liquid state at 795 °C. At the same time, the MoO_3 is gradually lost to the current, and completely disappears at about 850 °C.

As for samples containing MoO_2 or Mo_4O_{11}, the recrystallization phenomenon will occur at higher temperatures, and some substances will be left on the thermocouple wire after roasting. The melting points of samples containing MoO_2 or Mo_4O_{11} were measured, as shown in Fig. 12. It is seen that the melting point of MoO_3-rich system can drop by 25−30 °C as 2.5 wt.% MoO_2 or 15 wt.% Mo_4O_{11} is introduced. However, when MoO_2 content is over 7.5 wt.% or Mo_4O_{11} content is over 30 wt.%, the system will have higher melting temperatures than pure MoO_3. Therefore, when MoO_2 and Mo_4O_{11} are newly formed, the melting

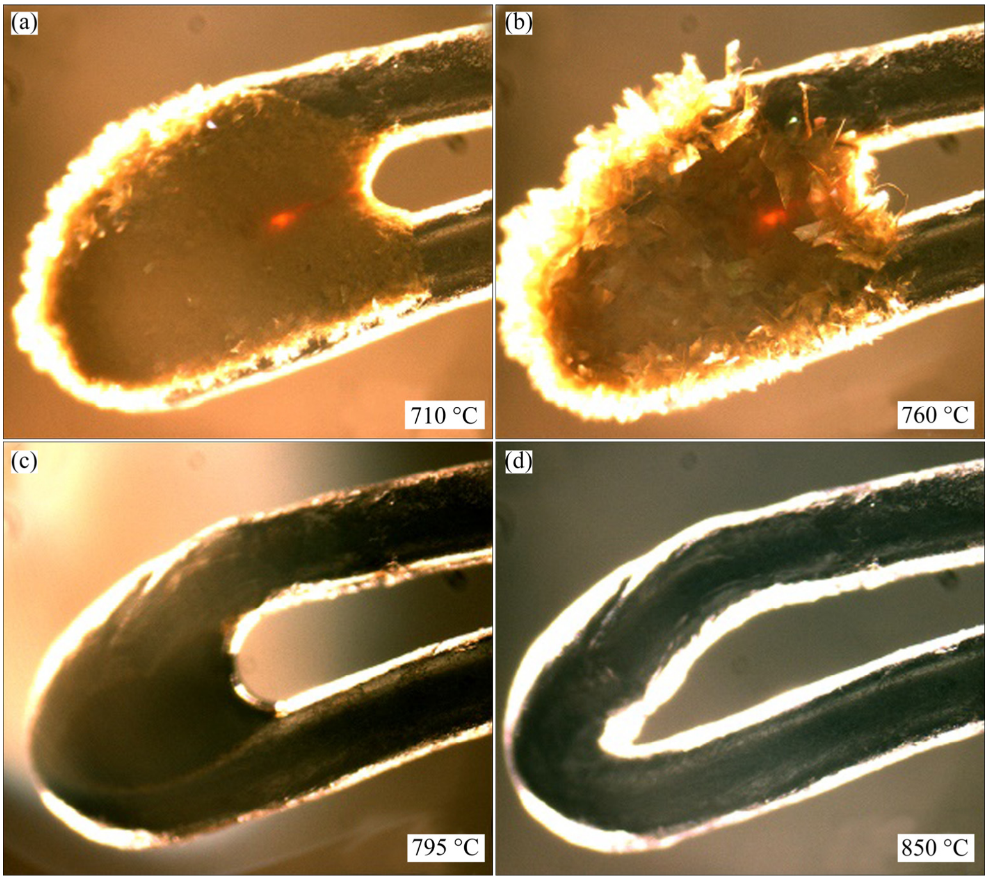

Fig. 11 Changes in states of pure MoO_3 loading on Pt−Rh thermocouple wire with heating temperature: (a, b) Recrystallization; (c) Complete melting; (d) Complete volatilization

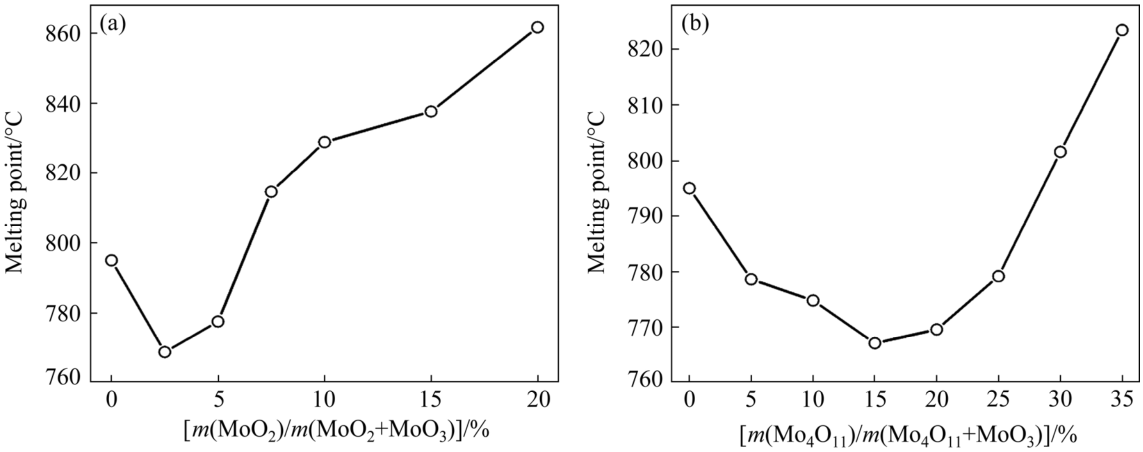

Fig. 12 Melting points of MoO_3−MoO_2 (a) and MoO_3−Mo_4O_{11} (b) systems

point of MoO_3-rich system will decrease and the liquid amount will increase; when contents of MoO_2 and Mo_4O_{11} reach certain levels, the melting points of MoO_3-rich systems begin to decrease, which promotes the solidification of liquid phase. Because the solidified layer has a very dense structure, the wrapped MoO_2 and Mo_4O_{11} are difficult to be oxidized even with the extending of roasting time.

Above results indicate that the initial stage of oxidative roasting should be carefully manipulated to avoid a large-area sintering. The measures including raising the temperature and oxygen content are undesirable. Instead, re-circulated flue gas with low O_2 content may work to prevent the exothermic oxidation from going on violently, and measures such as accelerating the movements of gas and ore may be useful to improve heat transfer to cold areas.

4 Conclusions

(1) The surface MoS_2 contacting O_2 tends to be directly oxidized into MoO_3 at the beginning of roasting, which locally brings about giant exothermic effect, thus leading to the formation of liquid MoO_3.

(2) The liquid MoO_3 can migrate into inner cracks, bind solid particles, and rapidly react with MoS_2 to form MoO_2 and Mo_4O_{11}. The MoO_2 and Mo_4O_{11} can also decrease the melting point of MoO_3-rich layer by as high as 25−30 °C. Hence, MoO_2 and Mo_4O_{11} are intensively formed and constitute the sintered layer at the beginning of roasting.

(3) A roasting temperature of 600 °C is high enough to cause the sintering of pellet surface that faces the air flow, while higher temperatures will result in larger sintered area, which even covers partial surface on the leeward side. Once the sintered surface is formed, it continuously inhibits oxidation process due to the block of inner paths for O_2 diffusion. Thus, MoS_2 pellets roasted at high temperatures over 650 °C are slowly oxidized at later stages.

Acknowledgments

This work was financially supported by the Basic Science Center Program of the National Natural Science Foundation of China (No. 72088101), the General Program of the National Natural Science Foundation of China (No. 51874355), and the Special Funding of China Postdoctoral Science Foundation (No. 2020T130730).

References

[1] ERIC R H. Treatise on process metallurgy [M]. Amsterdam: Elsevier, 2014.

[2] GASIK M, DASHEVSKII V, BIZHANOV A. Ferroalloys [M]. Berlin: Springer, 2020.

[3] BRAITHWAITE E R, HABER J. Molybdenum: An outline of its chemistry and uses [M]. Amsterdam: Elsevier, 2013.

[4] XIANG Tie-gen. Molybdenum metallurgy [M]. Changsha: Central South University Press, 2002. (in Chinese)

[5] SUN Hu, LI Guang-hui, YU Jun-jie, LUO Jun, RAO Ming-jun, PENG Zhi-wei, ZHANG Yuan-bo, JIANG Tao. Preparation of high purity MoO_3 through volatilization of technical-grade Mo calcine in water vapor atmosphere [J]. International Journal of Refractory Metals and Hard Materials, 2018, 77: 1−7.

[6] LI Guang-hui, BU Qun-zhen, SUN Hu, SHI Da-peng, LUO Jun, RAO Ming-jun, PENG Zhi-wei, JIANG Tao. Cost-effective and sustainable preparation of porous mullite-based ceramics combining MoO_3 recovery from industrial calcine [J]. ACS Sustainable Chemistry & Engineering, 2020, 8(19): 7290−7299.

[7] FU Yun-feng, XIAO Qing-gui, GAO Yi-ying, NING Peng-ge, XU Hong-bin, ZHANG Yi. Pressure aqueous oxidation of molybdenite concentrate with oxygen [J]. Hydrometallurgy, 2017, 174: 131−139.

[8] LASHEEN T A, EL-AHMADY M E, HASSIB H B, HELAL A S. Molybdenum metallurgy review: Hydrometallurgical routes to recovery of molybdenum from ores and mineral raw materials [J]. Mineral Processing and Extractive Metallurgy Review, 2015, 36(3): 145−173.

[9] FENG Dan-dan. Analysis and prospect of supply and demand situation of glogal molybdenum resources [J]. Land and Resources Information, 2020(10): 39−44. (in Chinese)

[10] HE Shu-rong. The practical techniques and the technical progress of techniexl molybdenum oxide production [J]. Development and Application of Materials, 2013, 28(1): 96−101. (in Chinese)

[11] AN Jing. Analsis of production technology and pollution treatment of technical-grade molybdenum oxide [J]. New Technology & New Products of China, 2016(23): 126−127. (in Chinese)

[12] DOHEIM M A, ABDEL-WAHAB M Z, RASSOUL S A. Fluidized bed roasting of molybdenite-effect of operating variables [J]. Metallurgical Transactions B, 1976, 7(3): 477−483.

[13] PALANT A A. Pelletizing of sulfide molybdenite concentrates [J]. Russian Metallurgy (Metally), 2007(2): 109−111.

[14] EBRAHIMI-KAHRIZSANGI R, ABBASI M H, SAIDI A. Mechanochemical effects on the molybdenite roasting

kinetics [J]. Chemical Engineering Journal, 2006, 121(2/3): 65−71.

[15] KIM B S, LEE H I, CHOI Y Y, KIM S B. Kinetics of the oxidative roasting of low grade Mongolian molybdenite concentrate [J]. Materials Transactions, 2009, 50(11): 2669−2674.

[16] LI Xiao-bin, WU Tao, ZHOU Qiu-sheng, QI Tian-gui, PENG Zhi-hong, LIU Gui-hua. Kinetics of oxidation roasting of molybdenite with different particle sizes [J]. Transactions of Nonferrous Metals Society of China, 2021, 31(3): 842−852.

[17] LI Guang-hui, YOU Zhi-xiong, SUN Hu, SUN Rong, PENG Zhi-wei, ZHANG Yuan-bo, JIANG Tao. Separation of rhenium from lead-rich molybdenite concentrate via hydrochloric acid leaching followed by oxidative roasting [J]. Metals, 2016, 6(11): 282.

[18] SUN Hu, LI Guang-hui, WANG Jian, BU Qun-zhen, LUO Jun, RAO Ming-jun, PENG Zhi-wei, JIANG Tao. Short-flow preparation of pure MoO_3 from $CaCO_3$-added molybdenite concentrate pellet by sublimation with flue gas recirculation [J]. Journal of Cleaner Production, 2021, 284: 124747.

[19] SUN Hu, LI Guang-hui, YU Jun-jie, LUO Jun, RAO Ming-jun, PENG Zhi-wei, JIANG Tao. A novel simultaneous oxidizing−volatilizing process for efficient separation of pure MoO_3 from structure self-sustained molybdenite concentrate pellets [J]. Powder Technology, 2019, 345: 338−345.

[20] WANG Lu, ZHANG Guo-hua, WANG Jing-song, CHOU K C. Influences of different components on agglomeration behavior of MoS_2 during oxidation roasting process in air [J]. Metallurgical and Materials Transactions B, 2016, 47(4): 2421−2432.

[21] UTIGARD T. Oxidation mechanism of molybdenite concentrate [J]. Metallurgical and Materials Transactions B, 2009, 40(4): 490−496.

[22] WANG Lu, ZHANG Guo-hua, DANG Jie, CHOU Kuo-chih. Oxidation of roasting of molybdenite concentrate [J]. Transactions of Nonferrous Metals Society of China, 2015, 25(12): 4167−4174.

[23] LIU Bing-bing, ZHANG Li, ZHANG Bei, WANG Jia, ZHANG Yuan-bo, HAN Gui-hong, CAO Yi-jun. Characterizations on phase reconstruction, microstructure evolution and separation of magnetic ferrite ceramics from low-grade manganese ores by novel uphill reaction diffusion and magnetic separation [J]. Materials Characterization, 2021, 175: 111028.

[24] SHIGEGAKI Y, BASU S K, WAKIHARA M, TANIGUCHI M. Thermal analysis and kinetics of oxidation of molybdenum sulfides [J]. Journal of Thermal Analysis, 1988, 34(5/6): 1427−1440.

[25] FAN Xiao-hui, DENG Qiong, GAN Min, CHEN Xu-ling. Roasting oxidation behaviors of ReS_2 and MoS_2 in powdery rhenium-bearing, low-grade molybdenum concentrate [J]. Transactions of Nonferrous Metals Society of China, 2019, 29(4): 840−848.

[26] DANG Jie, ZHANG Guo-hua, CHOU Kuo-chih, REDDY R G, HE Yu, SUN Yuan-jun. Kinetics and mechanism of hydrogen reduction of MoO_3 to MoO_2 [J]. International Journal of Refractory Metals and Hard Materials, 2013, 41: 216−223.

辉钼矿氧化焙烧自烧结的特点与机制

孙虎[1,2]，李光辉[1,2]，卜群真[1,2]，傅中乔[1,2]，刘会波[1,2]，张鑫[1,2]，罗骏[1,2]，饶明军[1,2]，姜涛[1,2]

1. 中南大学 资源加工与生物工程学院，长沙 410083；
2. 难冶有色金属资源高效利用国家工程实验室，长沙 410083

摘　要：以纯试剂为原料进行焙烧试验，采用热力学计算、XRD、SEM-EDS、高温原位分析等手段，研究辉钼矿(MoS_2)氧化过程的自烧结行为。结果表明，当焙烧温度由 600 °C 提高至 700 °C 时，辉钼矿团块中物料烧结的面积随之增大，导致脱硫效率降低。烧结层在氧化焙烧的初期快速形成，且常覆盖在团块迎风侧表面。在物料烧结的同时，MoO_2 和 Mo_4O_{11} 也集中生成，与 MoO_3 共同构成烧结层。进一步研究发现，含低价钼氧化物的富 MoO_3 产物熔点较低，在 MoS_2 与 O_2 反应剧烈放热时易发生熔化，致使物料烧结。

关键词：辉钼矿；氧化焙烧；烧结；分布特征；机制

(Edited by Wei-ping CHEN)